CHAPTER 44

FIELD VERIFICATION OF NUMERICAL MODELS FOR CALCULATION OF NEARSHORE WAVE FIELD

Takuzo Shimizu [1], Akiyuki Ukai [1] and Masahiko Isobe [2]

ABSTRACT

Field applicabilities of both the parabolic equation model and the energy flux equation model are verified through comaprisons with field data. The results show that the parabolic equation model has fairly good accuracy for estimating the wave height distribution of the actual wave field over a complex bottom topography, but the transformation of directional wave spectra cannot be reproduced satisfactorily in the surf zone. It is also found that the energy flux equation model is applicable for practical use although its basic equation has a shortcoming of not taking into account the diffraction in a strict sense.

INTRODUCTION

In recent years, a numerical predictive model of three-dimensional beach topography change has been developed and applied to many practical problems in Japan. A few attempts have been made to demonstrate the practical applicability of the model through comparisons of the numerical predictions with the actual topographical changes around a harbor (e.g. Shimizu et al. 1990). In order to properly predict the beach evolution due to construction of a coastal structure, it is first of all important to evaluate the wave field with good accuracy. In a numerical model for estimating the wave field in the nearshore region, wave transformation such as shoaling, refraction, diffraction and wave breaking should be taken into account. Moreover, treatment of random waves is important for the field application. In this study, two calculation models are examined; namely,

[1]Penta-Ocean Construction Co. Ltd. , 2-2-8 Koraku, Bunkyo-ku, Tokyo 112, Japan.
[2]Pfofessor, Dept. of Civil Eng., Univ. of Tokyo, 7-3-1 Hongo, Bunkyo-ku, Tokyo 113, Japan.

the wave energy flux equation model as described with the directional wave spectrum proposed by Karlsson(1969) and the parabolic-type equation model derived from the mild slope equation by using the wave ray-front coordinates proposed by Isobe(1987). We try to verify the field applicability of these two models quantitatively, through comparisons with the field measurement data. We shall also investigate the effects of the calculation results of the wave field on those of the wave-induced nearshore current field.

FIELD INVESTIGATION

The field verification of the models has not been thoroughly discussed owing to difficulties of obtaining field data on nearshore waves and currents under severe wave conditions. The field observation was, therefore, carried out around the Tomioka Fishery Harbor, facing directly the Pacific Ocean, Fukushima Prefecture, Japan. The Tomioka Fishery Harbor is under construction and has been troubled with harbor shoaling since the construction started in 1986.

Fig. 1 shows the bottom topography of the investigation site and the locations of observation points. The calculation area is the same as shown in this figure and is about 2.5 km long in the alongshore direction and about 1.5 km long in the cross-shore direction. The calculated wave rays by Snell's law are also shown in this figure. The wave rays are calculated for the mean wave condition of storm waves which attacked during the observation. The significant wave period is 8.6 seconds and the direction of the crestline is 6 degree oblique to the shoreline. The bottom contours are complex and there exist some rocky shoals. In the southeast of the harbor entrance, the bottom contours extend offshoreward like a tongue and the wave rays converge and intersect with each other around this shoal.

At six points in the nearshore region with the water depth of about 5 m, waves and nearshore currents were measured by using a combination of an ultrasonic wave gauge and an electro-magnetic current meter with a pressure sensor. The incident wave conditions were also measured at Point 0 with the water depth of 12 m. Synchronized measurements of the water surface elevation and the two components of horizontal water particle velocities were conducted. The measuring instruments have the self-recording system and had been placed on the seabed during the observation. 10-minutes measurements with the sampling time of 0.5 seconds were recorded on the magnetic casette tape every 2 hours for approximately one month.

The data obtained by an ultrasonic wave gauge during the storm waves beyond approximately 2 m are not normal because of intrusion of air bubbles due to wave breaking. The pressure fluctuations obtained by a pressure sensor are, therefore, converted into the water surface motion on the basis of the small amplitude wave theory. First, the pressure fluctuation profile is decomposed into a finite number of Fourier series components with the aid of the Fast Fourier Ttransform algorithm. The Fourier coefficients of the pressure flucutations are converted into those of the water surface fluctuations on the basis of the linear wave theory. The wave profile is, then, reconstructed with these converted Fourier coefficients

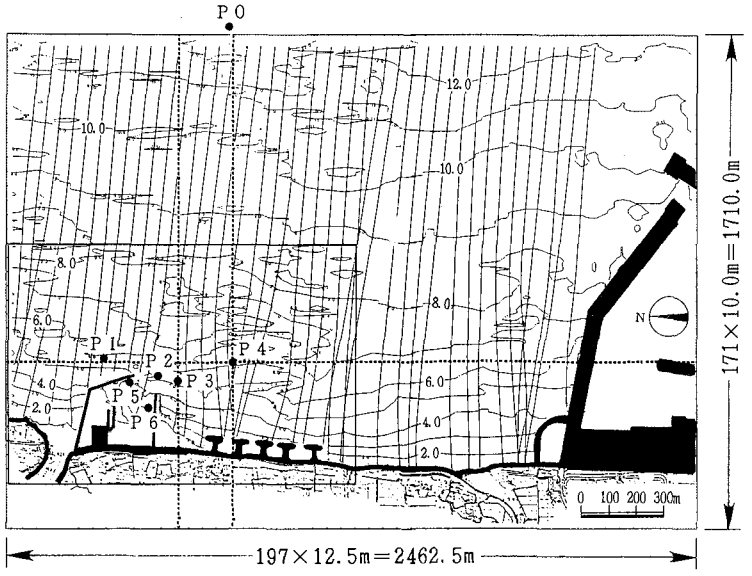

Fig. 1. Bottom topogaraphy of investigation site.

of water surface motion in the frequency range from 0.03 to 0.3 Hz. Moreover, the wave profiles estimated by using the pressure data are compared with those observed directly by the ultrasonic wave gauge during the relatively calm period when the simultaneous records of both data were obtained successfully.

The field observation was carried out over a period of approximately one month from September to November in 1990. During the observation, fortunately, storm waves greater than 3 m in significant wave height attacked twice. Our intrests are focussed on the data obtained at Point 4 where the increase in wave height is a result of refraction and diffraction effects due to bottom topography, and at Point 5 where diffraction behind the breakwater occurs.

CALCULATION METHOD

Energy Flux Equation Model (EFEM)

The wave energy flux equation model as described with the directional wave spectrum proposed by Karlsson(1969) has been widely used for refraction of random waves. In this study, the model with an additional term of energy dissipation is employed.

$$\frac{\partial}{\partial x}(Dv_x) + \frac{\partial}{\partial y}(Dv_y) + \frac{\partial}{\partial \theta}(Dv_\theta) = -f_D D \tag{1}$$

$$v_x = c_g \cos\theta, \quad v_y = c_g \sin\theta, \quad v_\theta = \left(\frac{c}{c_g}\right)\left(\frac{\partial c}{\partial x}\sin\theta - \frac{\partial c}{\partial y}\cos\theta\right) \tag{2}$$

where $D(f,\theta)$ is the directional wave spectrum, c_g the group velocity, c the wave celerity and f_D the energy dissipation coeffcient.

In this model, random waves are treated directly as the directional wave spectrum. Therefore, this model has an advantage of the computational time being relatively short in a wide region such as the actual field. On the other hand, this equation has a shortcoming of not taking the diffraction into account in a strict sense. But, this model gives an approximate estimation of diffracted wave height for practical applications, because diffraction of random waves can be explained mainly by the directional spreading.

Parabolic Equation Model (PEM)

Many numerical models for calculation of the wave field under combined refraction and diffraction above a complex bottom topography have been developed on the basis of the mild slope equation. Approximate parabolic-type equations are often adopted because much computational time can be saved owing to the forward stepping scheme.

Isobe(1987) developed a parabolic equation model for the random waves transformation due to refraction, diffraction and wave breaking. Irregular waves are described as a superposition of component regular waves with different frequencies and directions. In order to improve the accuracy of calculating the wave transformation for a wide range of propagation directions of component waves, a curvilinear coordinate system is introduced and the parabolic equation is derived by taking into account the difference between directions of wave propagation and a pre-chosen coordinate. This coordinate consists of wave rays and fronts for modified bottom topography in which wave rays do not intersect with each other. In this model, the curvilinear coordinates are defined from the peak wave frequency and peak direction of the directional spectrum. In a shadow region, additional wave rays are radiated from the tip of the breakwater.

The following parabolic-type approximate equation was derived in the curvilinear coordinate system.

$$\frac{1}{Gh_\xi}\frac{1}{h_\eta}\frac{\partial}{\partial\eta}\left(G\frac{h_\xi}{h_\eta}\frac{\partial\phi}{\partial\eta}\right)+2ik_\xi\frac{1}{h_\xi}\frac{\partial\phi}{\partial\xi} + \left\{\frac{i}{Gh_\eta}\frac{1}{h_\xi}\frac{\partial(k_\xi Gh_\eta)}{\partial\xi}+(k^2+{k_\xi}^2)+i\frac{\omega}{G}f_D\right\}\phi=0 \quad (3)$$

where ϕ is the complex amplitude of water surface fluctuation, $G=cc_g$, ω the angular frequency, k the wave number, k_ξ the ξ-direction component of the wave number vector, and h_ξ and h_η the ξ- and η -direction scale factors of the curvilinear coordinates, respectively.

Energy Dissipation Model

As for the energy dissipation term due to wave breaking, the model proposed by Isobe(1987) is employed in both models. This energy dissipation model is devided into two phases. The first phase is the determination of breaking point

and the second is the evaluation of energy dissipation coefficient. The breaker index of an individual wave is expressed by the ratio of water particle velocity to wave celerity as follows.

$$\gamma_b' \equiv (\hat{u}/c)_b$$
$$= 0.53 - 0.3\exp\left\{-3\sqrt{d_b/L_0}\right\} + 5\tan^{3/2}\beta\exp\left\{-45\left(\sqrt{d_b/L_0} - 0.1\right)^2\right\} \quad (4)$$

where γ_b' is the criterion for regular waves, u the amplitude of horizontal water particle velocity at still water level, d the water depth, L_0 the deepwater wavelength, $\tan\beta$ the bottom slope, and the subscript b denotes quantities at the breaking point.

The ratio at the breaking point for individual waves of an irregular wave train was temporally taken as 0.8 times that for regular waves in the original paper. In this study, through comparisons with feld measurement data, the coefficient is assumed to be 0.7. The breaker index for random waves, γ_b, is indicated as follows.

$$\gamma_b = 0.7\gamma_b' \quad (5)$$

The energy dissipation coefficient of irregular waves is given as the product of the probability of breaking waves and the energy dissipation coefficient of regular waves.

$$f_D = P_B f_D' \quad (6)$$

where f_D is the energy dissipation coefficient of irregular waves, P_B the probability of breaking waves, and f_D' the energy dissipation coefficient of regular waves.

$$f_D' = -\frac{5}{2}\sqrt{\frac{g}{d}}\sqrt{\frac{\gamma - \gamma_r}{\gamma_s - \gamma_r}}f_d(kd)\tan\beta \quad (7)$$

$$f_d(kd) = \sqrt{\frac{\tanh kd}{kd}}\frac{1}{2}(1+s_2)\left\{1 - \frac{5(1-s_2)(1+s_2) + 2s_2(s_2\cosh 2kd - 1)}{5(1+s_2)^2}\right\} \quad (8)$$

$$s_2 = 2kd/\sinh 2kd \quad (9)$$

$$\gamma_s = 0.4 \times (0.57 + 5.3\tan\beta) \quad (10)$$

$$\gamma_r = 0.135 \quad (11)$$

where γ_s and γ_r give the maximum values of γ on a uniform slope and in the wave recovery zone respectively. Eq.(7) to (9) are evaluated by using the significant wave as a representative wave.

On the assumption of the Rayleigh distribution, the probability of breaking waves is expressed as follows.

$$P_B = \left\{1 + 2.004\left(\frac{\gamma_b}{\tilde{\gamma}_{1/3}}\right)^2\right\}\exp\left[-2.004\left(\frac{\gamma_b}{\tilde{\gamma}_{1/3}}\right)^2\right] \quad (12)$$

where $\tilde{\gamma}_{1/3}$ is the value of γ without breaking dissipation corresponding to the significant wave. Both the energy equation model and the parabolic equation model are based on the small amplitude wave theory. However, the effect of wave nonlinearity cannot be neglected in the shallow water. Here, the nonlinearity effect is treated by multiplying a correction factor to the wave height. For non-breaking waves, the first-order cnoidal wave theory is used (Isobe, 1985) and for breaking waves, the correction factor is taken to be 1.25 on the basis of experimental results.

COMPARISON OF WAVE HEIGHT AND DIRECTION

The parabolic equation method and the energy flux equation method were applied to reproduction of the observed wave field. In order to compare the calculations with the measurements, the measurement data obtained at Point 0 are classified into three cases in accordance with the wave height level. The wave direction is limitted to the predominant direction, E. The numerical calculations are conducted for the mean significant waves of these three classifications, using the Bretschneider-Mitsuyasu frequency spectrum and the Mitsuyasu-type directional spreading function. The directional spreading parameter S_{max} is set to be 25, because the observed values at Point 0 were about 20 to 30 during the observation. The numbers of frequency and directional intervals with equal spacing are 10 and 15 respectively for calculation by the parabolic equation model, and 10 and 45 for that by the energy equation model.

Fig. 2(a) and (b) show the calculated wave fields for regular waves and for irregular waves by the parabolic equation model. The incident significant wave height is 2.9 m, the significant wave period is 8.5 s and the wave direction is E. As seen in Fig. 2(a) for regular waves, the extraordinary spatial variations in wave height are calculated owing to refraction over the complicated bottom topography. The calculation for random waves, on the other hand, show rather smooth wave height distribution because of presence of various directional and frequency components. Fig. 2(c) is the calculation result by the energy flux equation model. The spatial variation in wave height is even smoother than that of the parabolic equation model. Judging from these results, treatment of random waves is seemed to be inevitable for field application.

Fig. 3 shows the relationship between the incident wave height at Point 0 and that at the representative observation point in the nearshore region. The scattered plots are the measurements and the symbols are the calculations. At Point 3 near the harbor entrance, the significant wave height is almost the same as the incident wave height under relatively calm waves and becomes a little smaller owing to the wave breaking when the incident wave height is beyond 2 m. At Point 4 around the rocky shoal, the wave height increases owing to refraction over the shoal compared with the incident wave heiglit, and the effect of wave breaking appear when the incident wave height becomes greater than 2 m. Altough the conventional refraction analysis of regular waves gives the crossing of wave rays, both of the computed results by the parabolic equation model and by the energy flux equation model show good agreements with the measurements. As it was

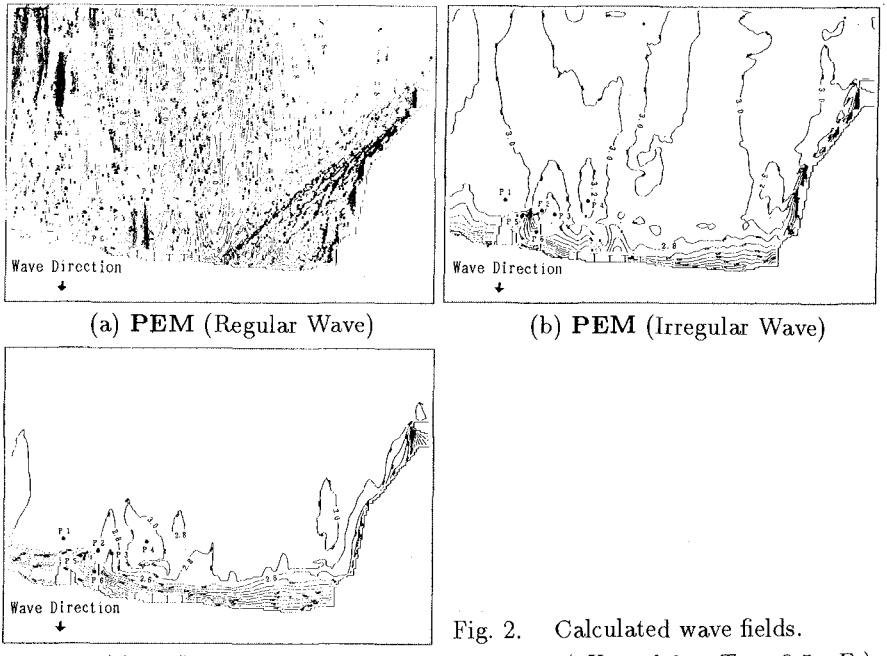

(a) **PEM** (Regular Wave)

(b) **PEM** (Irregular Wave)

(c) **EFEM**

Fig. 2. Calculated wave fields.
($H_{1/3}$=2.9m, $T_{1/3}$=8.5s, E)

expected at Point 5, in the sheltering area behind the breakwater, the results calculated by the energy flux equation model underestimate the measurements. On the other hand, the calculated results by the parabolic equation model show fairly good agreements with the measurements.

Fig. 4 shows the comparisons between the measured and the calculated significant wave heights including data at Point 1 and 2. The calculations of the parbolic equation model agree with the measurements much better than those of the energy flux equation model.

Fig. 5 shows the comparisons between the measured and the calculated principal directions. The calculations of both the parabolic equation model and the energy flux equation model for irregular waves agree fairly well with the measurements.

COMPARISON OF DIRECTIONAL WAVE SPECTRUM

Measured Directional Wave Spectra

The directional wave spectra were estimated by the Maximum Entropy Method (MEP ; Kobune and Hashimoto, 1986). The Maximum Entropy Method has an

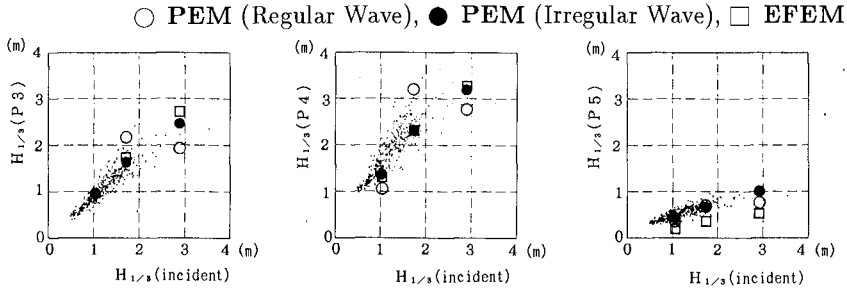

(a) Point 3 (b) Point 4 (b) Point 5

Fig. 3. Relationship between incident wave height at Point 0 and that at representative observation point.

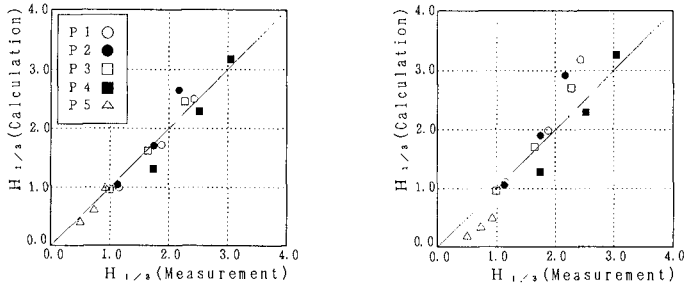

(a) **PEM** (Irregular Wave) (b) **EFEM**

Fig. 4. Comparisons between the measured and the calculated significant wave heights.

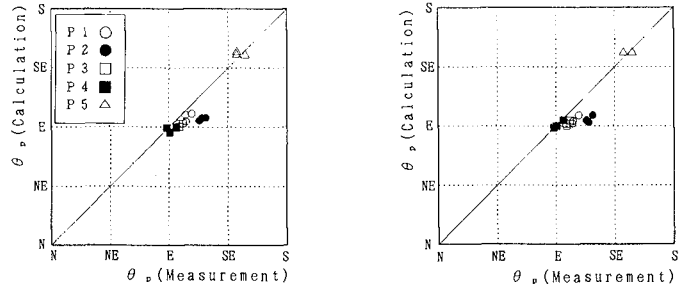

(a) **PEM** (Irregular Wave) (b) **EFEM**

Fig. 5. Comparisons between the measured and the calculated principal directions.

extremely high resolution for a three sensor array. In this study, the pressure fluctuation measured by a pressure sensor and the two components of the horizontal water particle velocities measured by an electromagnetic current meter are used for estimating the directional wave spectrum. The directional spreading parameter S of the Mitsuyasu-type directional distribution function can be estimated as a function of frequency as follows (e.g. Isobe, 1988).

$$S(f) = \left(\frac{1}{\gamma(f)^2} - \frac{1}{2}\right) + \left(\frac{1}{\gamma(f)^4} - \frac{3}{4}\right)^{1/2} \tag{13}$$

The frequency-dependent longcrestedness parameter, $\gamma(f)$, can be evaluated by eq.(14) and (15) and using the estimated directional spectrum.

$$\gamma(f) = \left\{\frac{M_{20} + M_{02} - \sqrt{(M_{20} - M_{02})^2 + 4M_{11}^2}}{M_{20} + M_{02} + \sqrt{(M_{20} - M_{02})^2 + 4M_{11}^2}}\right\}^{1/2} \tag{14}$$

$$M_{pq}(f) = \int_{\theta_p - \frac{\pi}{2}}^{\theta_p + \frac{\pi}{2}} D(f,\theta) k^{p+q} \cos^p\theta \sin^q\theta d\theta \tag{15}$$

where θ_p is the angle at the spectral peak.

Fig. 6(a) shows the observed frequeny spectra and frequency-dependent directional spreading parameters under non-breaking wave condition with an incident significant wave height of 0.92 m and its period of 6.95 s, and (b) shows those under breaking wave condition with corresponding values of 3.21 m and 7.6 s. The frequency spectra observed at Point 3 and 4 in the nearshore region, have higher energy densities in both low and high freuency regions than those observed at Point 0. This tendency is remarkable under the severer wave condition as shown in Fig. 6(b). The high frequency fluctuations are due to wave breaking and the long-period motions are due to surf beats. Under the relatively calm condition, as shown in Fig. 6(a), the peakedness of directional wave spectrum increases owing to refraction at Point 3 near the harbor entrance compared with that at Point 0. On the contrary, as can be seen from Fig. 6(b), under the severe wave condition the peakedness does not increase. At Point 4 around the shoal, the peakedness does not increase owing to the intersection of wave rays under both conditions.

Fig. 7 shows the observed relations between the incident significant wave height and two ratios at the two points; one is the ratio of the significant wave height to the incident wave height and the other is the ratio of the directional spreading parameter of the peak frequency to that of the incident waves. Under the non-breaking condition where the significant wave height is below 2 m, at Point 3 near the harbor entrance as indicated schematically by the dash line, the peakedness of the directional distribution function increases owing to refraction compared with that of the incident wave. This can be usually seen in an area where the seabed topography has straight and parallel depth contours. At Point 4 around the shoal as illustrated by the solid line, the directional spreading parameter does not increase and is nearly equal to that of the incident wave, although

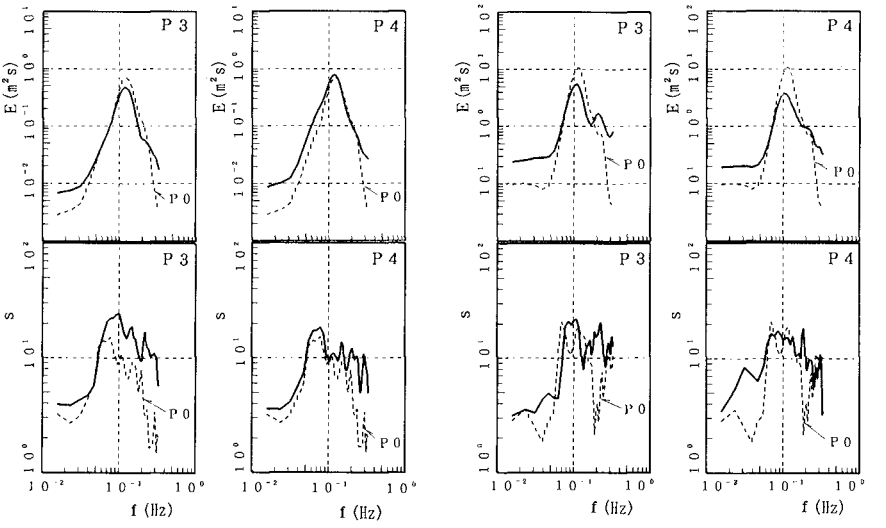

(a) Non-breaking wave condition (b) Breaking wave condition

Fig. 6. Observed frequency spectra and frequency-dependent directional spreading parameters.

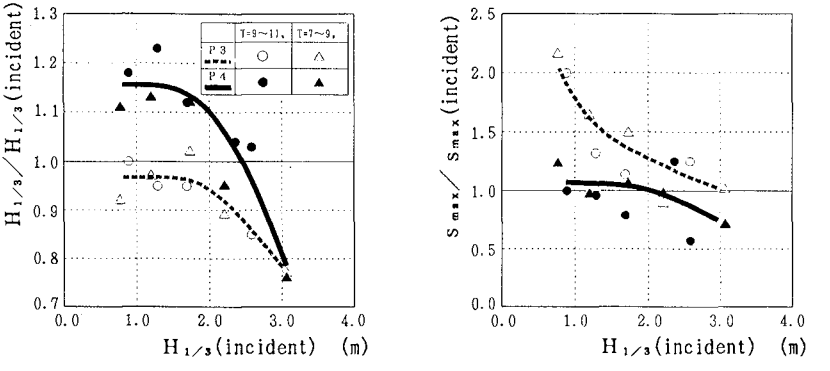

(a) (b)

Fig. 7. Observed relations between incident significant wave height and two ratios; (a) the ratio of the significant wave height to the incident wave height and (b) the ratio of the directional spreading parameter of the peak frequency to that of the incident waves.

the wave height increases owing to refration. In fact, because of the intersection of wave rays, the diffraction effect due to bottom topography occurs. Under the stormy wave conditions where the significant wave height is beyond 2 m, the directional spreading parameter at Point 3 decreases and is approximately equal to that at Point 4 around the shoal. This is supposed to be caused by wave breaking.

Comparison between Calculations and Measurements

Fig. 8 shows comparisons between the measured and the calculated directional distribution functions which are integrated with respect to frequency. The calculations are conducted for the severest wave condition during the observation. The significant wave height is 3.5 m and the significant wave period 8.5 s. Under this condition, the observation points in the nearshore region were included in the surf zone. At Point 3 near the entrance of the harbor, both the results of the parabolic equation model and the energy flux equation model give larger peakedness than the measurements. At Point 4 behind the shoal, it is reproduced qualitatively that the calculated directional distribution functions have a smaller peakedness than those at Point 3. But the results of the energy flux equation model show better agreement with the measurements than that of the parabolic equation model. At Point 5 behind the breakwater, according to the results by the parabolic equation model, an extremely sharp directional distribution function is calculated of which the spectral peak direction is on a line from the tip of the breakwater to the observation point. The measured peakedness is, on the other hand, considerably dull and is close to the one calculated by the energy equation model. Although in the energy flux equation model diffraction cannot be taken into account, but the directional spreading is considered and there exists also a numerical diffusion especially in calculating the directional convection.

Fig. 9 shows the comparisons between the measured and the calculated frequency-dependent directional spreading parameter of the Mitsuyasu-type directional distribution function. Around the peak frequency of 0.12 Hz, the same tendencies are seen as shown in Fig. 8. It is a cynical result that the measured directional spectrum transformation in the nearshore region is reproduced seemingly better by the energy flux equation model, although the parbolic equation has theoretically good accuracy for calculating combined refraction and diffraction over a complicated bottom topography and behind a breakwater. There are some reasons for disagreement between the calculations by the parabolic equation and the field measurements in the surf zone. The first reason is that the parabolic equation model is based on the linear wave theory, but the actual waves are nonlinear in the surf zone. The second reason is that the energy dissipation model used in this study is a model for estimating the total energy transformation due to wave breaking and that the energy dissipation coefficient is assumed to be constant irrelevantly to the direction. Namely, it is assumed that the directional spectral shape does not change after wave breaking, which seems to be unrealistic. The other reason is that the method for estimating the directional wave spectrum is

$$G(\theta) = \int_0^\infty G'(f,\theta)\, df \,, \quad D(f,\theta) = S(f)\, G'(f,\theta)$$

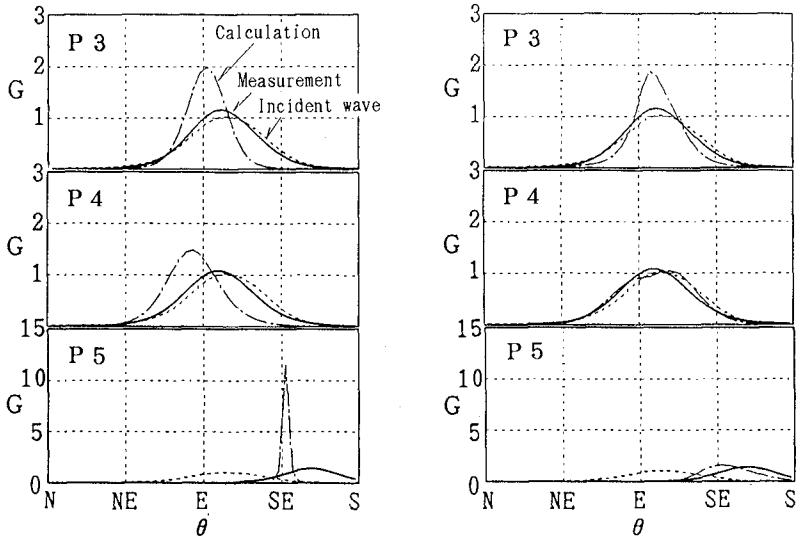

(a) **PEM** (Irregular Wave) (b) **EFEM**

Fig. 8. Comparisons between the measured and the calculated directional distribution functions.

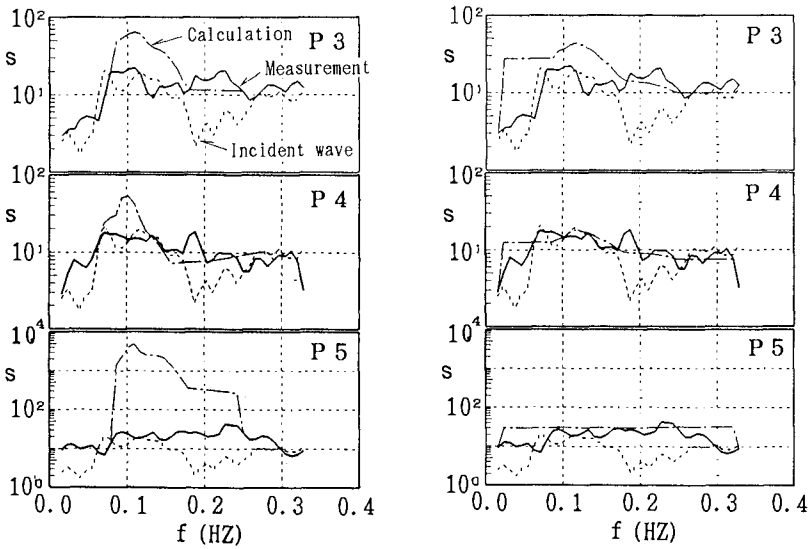

(a) **PEM** (Irregular Wave) (b) **EFEM**

Fig. 9. Comparisons between the measured and the calculated frequency-dependent directional spreading parameters.

also based on the linear wave theory, and therefore, it does not have high resolution for data measured in the surf zone. Thus, there remains rooms for improving the estimation method of the directional spectrum by taking into account nonlinearity of the actual sea state in the surf zone.

INFLUENCES ON NEARSHORE CURRENT FIELD

Finally, we attempt to investigate the effects of the calculation results of the wave field on those of the wave-induced nearshore current field. Fig. 10 shows the results of the nearshore current calculations. The measured velocity vectors are also illustrated, but in a different scale from the calculated vectors. Fig. 10(a) and (b) show the results for regular waves and for random waves by the parabolic equation model and (c) shows the results by the energy flux equation model. In computing the nearshore current field of random waves, the radiation stress is evaluated as for a regular wave with the equivalent wave energy and the principal direction which are estimated from the calculated directional wave spectrum. The group velocity and the wave celerity are estimated by using the significant wave period.

The result for regular waves gives an extremely large spatial variation and a strong shoreward current is calculated around the shoal in accordance with the spatial variation in wave height. On the other hand, the calculations by both

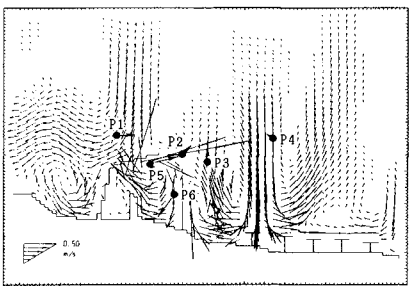

(a) **PEM** (Regular Wave)

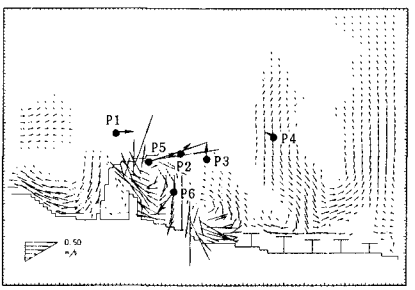

(b) **PEM** (Irregular Wave)

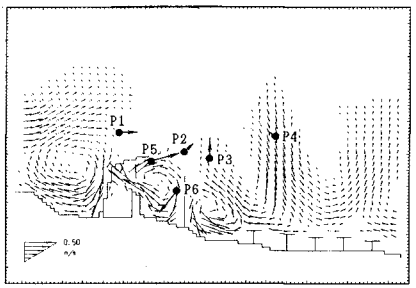

(c) **EFEM**

Fig. 10. Calculated current fields.

models for random waves show relatively smooth current fields. The observed dominant current pattern is reproduced satisfactorily. Thus, the current field calculation results are not so sensitive to the difference in the wave field calculation results if random waves are treated in the wave calculation model.

CONCLUDING REMARKS

The parabolic equation model and the energy flux equation model are applied to the calculation of the actual wave field over a complicated bottom topography and their field applicabilities are investigated through comparisons with the field data. As a result, it is found that both the parabolic equation model and the energy flux equation model are applicable for practical use and that the former has extremely good accuracy for estimating the wave energy transformation over a shoal, where the increase in wave height due to refraction and the diffraction effect due to bottom topography occur, as well as behind a breakwater. The transformation of directional wave spectra due to refraction and diffraction in the surf zone can be reproduced qualitatively by the parabilic equation model, but the observed directional spectra show smaller peakedness of the directional spreading function than the calculated ones. The observed spectra can be estimated better by the energy flux equation model. This is, however, a seeming agreement due to numerical diffusion. In order to properly estimate the transformation of directional wave spectra, it is necessary to accumulate further field data in the surf zone with good accuracy. It is also needed to develop a wave transformation model in which wave nonlinearity can be taken into account.

REFERENCES

Isobe, M., 1985: Calculation and application of first-order cnoidal wave theory, *Coastal Eng.* , Vol. 9, pp.309-325.

Isobe, M., 1987: A parabolic equation model for transformation of irregular waves due to refraction, diffraction and breaking, *Coastal Eng. in Japan*, Vol. 30, No. 1, JSCE, pp.33-47.

Isobe, M., 1988: Spectral description of irregular waves, *Nearshore Dynamics and Coastal Processes*, K. Horikawa (ed.), Univ. of Tokyo Press, pp.35-44.

Kobune, K. and N. Hashimoto, 1986: Estimation of directional spectra from the maximum entropy principle, *Proc. 5th Offshore Mechanics and Arctic Eng. Symposium*, Vol. I, ASME, pp.80-85.

Shimizu, T., H. Nodani and K. Kondo, 1990: Practical application of the three-dimensional beach evolution model, *Proc. 22nd Coastal Eng. Conf.*, ASCE, pp.2481-2494.